Fermion-mediated interactions in a dilute Bose-Einstein condensate

D. H. Santamore[1,2] and Eddy Timmermans[3]
[1]*T-4, Theoretical Division, Los Alamos National Laboratory, Los Alamos, New Mexico 87545, USA*
[2]*Department of Physics, Temple University, Philadelphia, Pennsylvania 19122, USA*
[3]*T-CNLS, Theoretical Division, Los Alamos National Laboratory, Los Alamos, New Mexico 87545, USA*
(Received 29 April 2008; published 17 July 2008)

We develop a diagrammatic perturbation treatment to calculate the zero-temperature equation of state of the dilute gas mixture of a single spin component Bose-Einstein condensate (BEC) and a normal Fermi gas of indistinguishable (single spin) fermion particles. We find that the mean-field description breaks down near the mechanical instability related to the phase separation phenomenon. Our analysis shows that the instability is caused by the competition of the usual short-range and fermion-mediated boson-boson interactions, which result in a boson compressibility that diverges. In the low BEC-density limit, we show that the diagrammatic analysis simplifies, we sum part of the higher-order diagrams, and we discuss the effects of other higher-order contributions.

DOI: 10.1103/PhysRevA.78.013619 PACS number(s): 03.75.Kk, 05.30.Jp, 67.90.+z

I. INTRODUCTION

Cold atom technology provides a novel laboratory for the many-body study of quantum liquids. In this paper, we focus on the low-temperature cold atom mixtures of dilute boson and fermion quantum liquids. The simultaneous trapping and cooling of fermionic and bosonic atoms has become a routine ingredient of the experimental cold atom repertoire. The original motivation for trapping these quantum gas mixtures was sympathetic cooling [1–3]: In the quantum degenerate regime, the standard evaporative cooling technique—the removal of the most energetic particles—is more efficient with bosonic than with fermionic atoms. Evaporatively cooled bosons, often a Bose-Einstein condensate (BEC), can subsequently cool the fermion particles by thermal contact.

In addition to its sympathetic cooling use, theorists also have pointed out intriguing prospects of cold atom technology for many-body studies: As the elementary BEC excitations are acoustic phonon modes, fermion-BEC mixtures consist of fermions interacting with a phonon fluid, thereby representing a large class of systems. A cold atom feature that is highly unusual in this broad context is the continuous tunability of the fermion-boson (and hence fermion-phonon) interactions, obtained by adjusting the strength of a homogeneous, external magnetic field—the Feshbach resonance. In general, the unprecedented accessibility, novel knobs, and probes suggest that in their role of prototypes of fermion-phonon fluid, the cold atom fermion-BEC mixtures can be used to break new ground by exploring polaronlike self-localization [4] or by measuring the rate of heat exchange between strongly coupled fermion-phonon fluids (temperature relaxation).

From the perspective of quantum liquid physics, a particularly relevant phenomenon is the phase-separation transition that the fermion-BEC mixture is expected to undergo as the fermion-boson interaction strength is increased [5]. This transition is the analogue of the phase separation of condensed ^{3}He-^{4}He fluid mixtures studied in traditional low-temperature physics [8]. As we describe in Sec. II, we expect the cold atom phase-separation transition to be first order [9], as was observed in the condensed-matter helium mixtures. Accessing this transition by varying the densities and/or the interaction strengths would allow the unusual, though highly relevant, experimental exploration of first-order (zero-temperature) quantum phase transitions. As a first-order transition, its dynamics can involve nucleation or a spinodal decomposition. At sufficiently low temperatures, the nucleation process cannot be triggered by thermal activation and has to proceed via a many-body tunneling process. Hence, the cold atom fermion-BEC mixtures promise the prospect of many-body tunneling studies, as well as investigations of first-order quantum phase transitions [10].

The focus of our work in this paper is the role of mediated interactions—the modification of the interactions of particles in one fluid caused by the presence of the other fluid. This phenomenon is of fundamental importance: fermionic particles interact via boson-field mediated interactions in the standard model. In the phase separation of low-temperature condensed helium mixtures, mediated interactions play a crucial role [11]. In those systems, the condensed ^{3}He fermion liquid remains "normal" (i.e., does not become superfluid) in the experimentally accessible regime, whereas the ^{4}He boson fluid can take on a BEC-like superfluid state. Boson mediated interactions are expected to make the fermions superfluid [12] as well, but at temperatures that are an order of magnitude lower than can be reached with present cooling technology. The condensed ^{3}He-^{4}He mixtures undergo phase separation when the fraction of fermion particles exceeds a minimal value: the system then breaks translational symmetry by forming local regions in which only fermion particles reside. While our understanding of these systems remains limited by the difficulties involved in accounting for strong interaction effects, theorists understood early on that the phase-separation phenomenon is triggered by mediated interactions [11]. Mean-field studies of the cold atom fermion-BEC mixtures indicated that these gas mixtures would similarly undergo phase separation under experimentally attainable conditions. Hence, it should be possible to study mediated interactions in a cold atom environment that is amenable to a first-principle description.

Mediated interactions stem from a particular type of correlations: the local density of the second fluid is altered near the position of a particle "1" of the first fluid, thereby changing the potential energy experienced by another, nearby particle "2" of the first fluid. However, most cold atom phase-separation studies have been carried out in the mean-field approximation, which neglects all correlations. Other studies neglected dominant contributions [13–15]. The zero-temperature equation of state and, hence, the density profile calculated within the mean-field equation of state cannot be expected to give a quantitatively correct description.

In Sec. II, we derive the equation of the state of the above system within the mean-field approximation. In Sec. III, we describe the fermion-mediated boson-boson interactions starting from linear-response theory. Then, we develop a general perturbation formalism that accounts for the relevant correlations in the following four sections, Secs. IV–VII. Our second-order calculation indicates that the instability associated with the spinodal decomposition is a saddle point instability, as predicted by the mean-field model, but is caused by the divergence of the BEC compressibility. In the low-density BEC limit, we find that the perturbation treatment simplifies and we show that higher-order terms significantly lower the fermion density of the instability point and make the instability line dependent upon the BEC density. From a partial summation of diagrams, we find an analytical expression for the equation of state and estimate the effect of other contributions.

II. COLD ATOM BACKGROUND AND MEAN-FIELD DESCRIPTION

In this section, we describe the ground state of a dilute gas mixture of single-component fermionic atoms and single spin projection bosonic atoms. These fermions (bosons), interacting via short-range atom-atom interaction potentials, are indistinguishable particles with mass m_F (m_B), distributed in space with average particle density $\rho_F^0(\mathbf{r})$ [$\rho_B^0(\mathbf{r})$]. We assume that the fermions are not paired into a superfluid, which may require the system to have a temperature above the critical temperature T_c for mediated interaction induced fermion pairing [6,7]. In practice, however, the T_c for such fermion pairing [16,17] is much lower than any other relevant energy scale so that there is a temperature regime in which for all practical purposes we can treat the unpaired fermion-BEC mixture as a zero-temperature system with a normal fermion fluid. Whether the p-wave pairing can be achieved may also depend on other factors: for instance, the inevitable loss processes that give a finite lifetime to the cold atom trap systems also heat up the system [18]. This is a process that will compete with the formation of any ultralow-temperature phase of matter.

As mentioned before, the mean-field description commonly used in cold atom physics neglects correlations and fluctuations in the expression of all expectation values. Accordingly, the interaction energy of this system, E_{int}, is approximated as

$$E_{\mathrm{int}} = \lambda_{BF} \int d^3r \rho_F^0(\mathbf{r}) \rho_B^0(\mathbf{r}) + \frac{\lambda_{BB}}{2} \int d^3r \rho_B^0(\mathbf{r}) \rho_B^0(\mathbf{r}), \quad (1)$$

where λ_{BF} and λ_{BB} are the interaction strengths with $\lambda_{BF} = 2\pi\hbar^2(m_F^{-1} + m_B^{-1})a_{BF}$ and $\lambda_{BB} = (4\pi\hbar^2/m_B)a_{BB}$, where a_{BF} and a_{BB} are the fermion-boson and boson-boson scattering lengths, respectively. We assume that the effective boson-boson interactions are repulsive, i.e., $a_{BB} > 0$, in order to have the system be mechanically stable.

Mølmer [19] pointed out that the trapped boson-fermion quantum gas mixtures can take on distinct spatial arrangements at low temperatures. When the fermion and boson particles mutually repel each other, $\lambda_{BF} > 0$, the mixtures can take on spatial configurations in which one region of space is occupied by only fermion particles, an arrangement akin to that of the phase-separated state in condensed ^{3}He-^{4}He mixtures. On the other hand, when the fermions and bosons attract each other, $\lambda_{BF} < 0$, the mutual attraction causes a density increase in the regions of fermion-boson overlap. If the attraction is sufficiently strong, the density increase leads to a collapsing instability [20] that was observed experimentally by Inguscio and co-workers [21].

In the mixtures of repulsive fermion-boson interaction, Viverit *et al.* [5] calculated the zero-temperature phase diagram in the mean-field approximation. Specifically, they discovered that the fermion-boson densities for an initially homogeneous mixture would take one of the following phases: (a) remain homogeneously mixed (phase I), (b) spatially separate into spatial regions of all fermion-gas and spatial regions containing a fermion-BEC mixture (phase II), and (c) separate into fermion-only and BEC-only regions (phase III). They have determined the density regime boundaries of the phase diagram by equating the mean-field pressures as well as the mean-field chemical potentials of those particles that reside in both kinds of spatial regions. The pressures and chemical potentials follow from the zero-temperature "equation of state:" the ground-state energy of a homogeneous mixture.

The mean-field equation of state of a homogeneous mixture of N_F fermions and N_B bosons confined to a macroscopic volume Ω, corresponding to average fermion and boson densities $\rho_F^0 = N_F/\Omega$ and $\rho_B^0 = N_B/\Omega$, respectively, is then equal to

$$E = \frac{\lambda_B N_B^2}{2\Omega} + \frac{\lambda_{BF} N_F N_B}{\Omega} + \frac{3}{5} \frac{\hbar^2 k_F^2 N_F}{2m_F}, \quad (2)$$

where k_F is the Fermi momentum $k_F = (6\pi^2\rho_F^0)^{1/3}$. Then, the fermion and boson chemical potentials, $\mu_B = dE/dN_B$ and $\mu_F = dE/dN_F$, follow from Eq. (2),

$$\mu_F = \frac{\hbar^2 k_F^2}{2m_F} + \lambda_{BF}\rho_B^0, \quad (3)$$

$$\mu_B = \lambda_{BB}\rho_B^0 + \lambda_{BF}\rho_F^0. \quad (4)$$

We obtain the same chemical potential equations by minimizing the free-energy function $F = E - \mu_B N_B - \mu_F N_F$ with respect to N_F and N_B. Note that the homogeneous mixture represents the physical ground state only if Eqs. (3) and (4) yield the global minimum of F. This global minimum condition requires that the second derivatives of F (or E) with respect to N_B and N_F be positive, i.e., $\partial\mu_B/\partial\rho_B^0 > 0$ and $\partial\mu_F/\partial\rho_F^0 > 0$. Physically, these mathematical conditions imply that the compressibility of the fermion and boson sys-

tems should be positive, as the isothermal compressibility, κ_j, is inversely proportional to the chemical potential derivative,

$$\kappa_j = -\frac{1}{\Omega}\left(\frac{\partial\Omega}{\partial P_j}\right)_T = \left[(\rho_j^0)^2\frac{\partial\mu_j}{\partial\rho_j}\right]^{-1}, \tag{5}$$

where P_j denotes the partial pressure experienced by gas j ($j=B$ or $j=F$), and where the subscript T indicates that the pressure derivative should be taken at constant temperature (zero temperature in this case). In addition, the condition of a global minimum also implies that the extremum cannot be a saddlepoint, which also requires $(\delta\mu_B/\partial\rho_F^0)^2 < (\partial\mu_B/\partial\rho_B^0)(\partial\mu_F/\partial\rho_F^0)$. Viverit *et al.* [5] noted that when the fermion density exceeds a critical value, $\rho_{F,\mathrm{crit}}$, where

$$\rho_{F,\mathrm{crit}} = \frac{3}{4\pi a_{BF}^3}\left[\frac{a_{BB}/a_{BF}}{(1+m_F/m_B)(1+m_B/m_F)}\right]^3, \tag{6}$$

the extremum is not a saddlepoint and the system can lower its energy by rolling down the saddlepoint in different N_B/N_F directions in different spatial regions. The "rolling down the saddlepoint" suggests a mechanism by which the mixture can phase-separate into regions of roughly equal size, i.e., undergo spinodal decomposition.

On the phase diagram in the boson fermion density plane, the line of spinodal decomposition, $\rho_F=\rho_{F,\mathrm{crit}}$, is located in the region with fermion densities above the phase I/II boundary [5]. Thus, one might wonder how the mixture phase-separates if the densities of the initial homogeneous mixture were located in between the I/II boundary line and the line of spinodal decomposition according to the mean-field description. We gain insight into this dynamics by plotting the free energy density $\mathcal{F}(\phi,\mu_F,\mu_B)=F/\Omega$ as a function of the superfluid BEC order parameter, which, if all bosons are Bose-condensed, is related to the boson density as $|\Phi|^2=\rho_B^0$. Actually, we find it useful to scale both the BEC order parameter as well as the free energy density. We introduce $|\Phi^0|$ with $|\Phi^0|^2=\mu_B/\lambda_{BB}$, and set $\phi=\Phi/|\Phi^0|$. We also define the scaled free energy by f, where $f=\mathcal{F}\lambda_{BB}/\mu_B^2$. Then, substituting the fermion density in terms of the fermion and boson chemical potentials, we obtain

$$f = \begin{cases} -|\phi|^2 + \frac{1}{2}|\phi|^4 - \alpha_{\mathrm{MF}}\left[1-\frac{|\phi|^2|}{\beta_{\mathrm{MF}}^2}\right]^{5/2} & \text{if } |\phi| < \beta_{\mathrm{MF}}, \\ -|\phi|^2 + \frac{1}{2}|\phi|^4 & \text{if } |\phi| > \beta_{\mathrm{MF}}. \end{cases} \tag{7}$$

where the dimensionless α_{MF} and β_{MF} parameters depend on the interaction parameters as well as on the chemical potentials,

$$\alpha_{\mathrm{MF}} = \frac{8}{3\pi}\left(\frac{m_F}{m_B}\right)[a_{BB}k_F^0(\mu_F)]\left(\frac{\mu_F}{\mu_B}\right)^2, \tag{8}$$

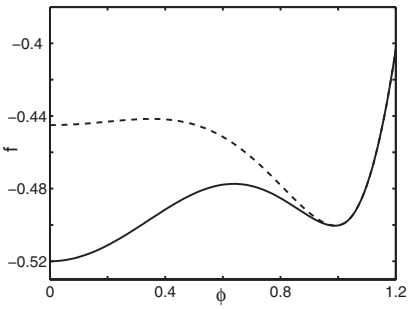

FIG. 1. Scaled free energy f as a function of ϕ [cf. Eq. (7)]. Dotted line shows the stable system (one global minimum) and solid line shows the system that can undergo first-order phase transition (one local minimum and one global minimum at the origin).

$$\beta_{\mathrm{MF}}^2 = \frac{\lambda_{BB}}{\lambda_{BF}}\frac{\mu_F}{\mu_B}, \tag{9}$$

and we have introduced an effective Fermi momentum, $k_F^0(\mu_F)=\sqrt{(2m_F/\hbar^2)\mu_F}$. In the density regime of interest (enclosed by the I/II phase boundary and the line of spinodal decomposition), the free energy (7) generally exhibits ϕ dependency as shown in Fig. 1. This shape of the Landau free energy is associated with a first-order phase transition: the system can reduce its free-energy by climbing or tunneling the free energy barrier that separates two local minima. In ordinary (finite-temperature) first-order phase transitions, thermal activation locally "pushes" the system over the barrier nucleating clumps of matter in the new phase. If the temperature is too low to initiate thermal activation, the system can penetrate the barrier and nucleate by quantum-mechanical tunneling [10]. The latter process, however, involves many-body tunneling, which the tunneling rate generally scales exponentially with the number of boson particles to be formed in each clump. A recent study [9] found that the tunneling rate exceeds the experimental lifetime of the system except very close to the line of spinodal decomposition or for very strong fermion-boson interactions. Otherwise, we can expect that at sufficiently low temperatures and below the line of spinodal decomposition, the fermion-boson mixture can remain in its homogeneous state for the duration of its experimental lifetime even if that homogeneous state represents a metastable equilibrium.

We are also interested in what the mean-field approximation predicts for the phase-separation dynamics in the spinodal decomposition region, $\rho_F^0 > \rho_{F,\mathrm{crit}}$. We can understand the linear onset of the instability dynamics from the study of the collective oscillations [22,23]. Our studies [24] revealed that two collective modes can be excited: a zero-sound mode with its sound velocity modified by boson-mediated fermion-fermion interactions, and a BEC sound mode modified by the fermion mediated boson-boson interactions. As the system approaches the line of spinodal decomposition, the fermion-mediated interactions reduce the BEC sound velocity. This velocity vanishes at the line and becomes imaginary above it, signaling the exponential growth of the long-wavelength modes. We have estimated the time scale on which the corresponding fluctuations (which drive the onset of the phase

dynamics) grow [25]. This analysis suggests that the fermion-mediated interactions make the BEC unstable. The vanishing of the sound velocity at the line of decomposition also suggests the divergence of the boson compressibility, as the compressibility is inversely proportional to the square of the sound velocity. However, the mean field equation of state does not exhibit this behavior. The mean field also fails to include polaron effects: the mass of a fermion particle immersed in a phonon-fluid can be significantly altered by its interactions with that fluid [26]. The importance of polaron effects was illustrated by a recent study [4] that showed a single impurity (a distinguishable atom immersed in a BEC) can self-localize into a small polaronlike state.

The rest of the paper deals with these problems by showing that the correlation physics which we will include in the calculation of the equation of state does lead to a divergence of the boson compressibility. The perturbation treatment that we develop in this paper includes polaron effects.

III. LINEAR-RESPONSE DESCRIPTION OF FERMION-MEDIATED BOSON-BOSON INTERACTIONS

In this section, we derive the fermion-mediated interaction effects up to lowest order by applying linear-response theory to a mean-field state. Writing the energy response of the homogeneous many-body system as the small-amplitude variation of the boson and fermion static densities, we obtain

$$\rho_B(\mathbf{r}) = \rho_B^0 + \delta\rho_B(\mathbf{r}), \tag{10}$$

$$\rho_F(\mathbf{r}) = \rho_F^0 + \delta\rho_F(\mathbf{r}). \tag{11}$$

We also determine the corresponding variation in the boson-boson interaction energy, $\delta E_{BB,\mathrm{int}}$, consistent with Eq. (1). To lowest order in the small-amplitude variation, the variation in interaction energy takes the form

$$\delta E_{BB,\mathrm{int}} = \int d^3r \int d^3r' \rho_B^0(\mathbf{r}) v_{BB,\mathrm{tot}}(\mathbf{r}-\mathbf{r}')\delta\rho_B(\mathbf{r}'), \tag{12}$$

and from this equation we will determine the "total" interparticle interaction potential, $v_{\mathrm{tot}}(\mathbf{r}-\mathbf{r}')$, that includes the fermion-mediated interaction potential, $v_{BB,\mathrm{fmed}}(\mathbf{r}-\mathbf{r}')$, in addition to the usual boson-boson contact interaction potential.

The boson density variation causes a modification of the overall mean-field potential experienced by the fermion particles, $\delta V_F(\mathbf{r})$, where

$$\delta V_F(\mathbf{r}) = \lambda_{BF}\delta\rho_B(\mathbf{r}). \tag{13}$$

In linear-response theory, the fermion density variation $\delta\rho_F(\mathbf{r})$ caused by the static fermion potential $\delta V_F(\mathbf{r})$ is determined by the static response function of the noninteracting fermions, χ_F^0,

$$\delta\rho_F(\mathbf{r}) = \int d^3r' \chi_F^0(\mathbf{r}-\mathbf{r}')\delta V_F(\mathbf{r}') = \lambda_{BF}\int d^3r' \chi_F^0(\mathbf{r}-\mathbf{r}')\delta\rho_B(\mathbf{r}'). \tag{14}$$

The above response function is the momentum Fourier transform of the dynamic response function $\chi_F^0(\mathbf{p},\omega)$ in the limit of vanishing frequency,

$$\chi_F^0(\mathbf{r}-\mathbf{r}') = \int d^3p \chi_F^0(\mathbf{p};\omega=0)\exp[i\mathbf{p}\cdot(\mathbf{r}-\mathbf{r}')]. \tag{15}$$

In general, the dynamic density-density response function of a system confined to a macroscopic volume Ω is

$$\chi_F(\mathbf{p},\omega) = \frac{1}{\Omega}\sum_{|\mathrm{int}\rangle} |{}_F\langle \mathrm{int}|\hat{\rho}_F(\mathbf{p})|0\rangle_F|^2 \times\left(\frac{1}{\hbar\omega-(E_{\mathrm{int}}-E_0)+i\eta}-\frac{1}{\hbar\omega+(E_{\mathrm{int}}-E_0)+i\eta}\right), \tag{16}$$

where $\hat{\rho}^F(\mathbf{p})$ denotes the Fourier transformed fermion density operator, E_0 represents the energy of the unperturbed ground state $|0\rangle$, and the summation runs over all intermediate excited fermion states $|\mathrm{int}\rangle$ of excitation energy $E_{\mathrm{int}}-E_0$. At the end of the calculation, we take the limit $\eta\to 0$ while approaching zero from the positive side $\eta>0$. In the static limit of a noninteracting fermion system for which the unperturbed ground state corresponds to a filled Fermi sphere and for which the intermediate states are particle-hole excitations, $\chi_F^0(\mathbf{p};\omega=0)$ yields

$$\chi_F^0(\mathbf{p};\omega=0) = -\frac{2}{\Omega}\sum_{|\mathrm{int}\rangle}\frac{n_{\mathbf{k}}^F(1-n_{\mathbf{k}+\mathbf{p}}^F)}{\epsilon_{\mathbf{k}+\mathbf{p}}^F-\epsilon_{\mathbf{k}}^F}, \tag{17}$$

where $\epsilon_{\mathbf{k}}^F$ is the excitation energy of a single fermion of momentum $\mathbf{k}$, and where $n_{\mathbf{k}}^F$ denotes the zero-temperature occupation number of the single-particle $\mathbf{k}$ momentum state. Then, the interaction energy caused by $\delta_{\rho B}$ and $\delta_{\rho F}$ is equal to

$$\delta E_{\mathrm{int}} = \int d^3r\rho_B^0(\mathbf{r})\lambda_{BB}\delta\rho_B(\mathbf{r}) + \int d^3r\rho_B^0(\mathbf{r})\lambda_{BF}\delta\rho_F(\mathbf{r}) + \int d^3r\rho_F^0(\mathbf{r})\lambda_{BF}\delta\rho_B(\mathbf{r}). \tag{18}$$

Inserting Eq. (14) into the mean-field energy of Eq. (18), we obtain the corresponding modification of the interaction energy,

$$\delta E_{\mathrm{int}} = \int d^3r\rho_B^0(\mathbf{r})\lambda_{BB}\delta\rho_B(\mathbf{r}) + \int d^3r\rho_F^0(\mathbf{r})\lambda_{BF}\delta\rho_B(\mathbf{r}) + \int d^3r\int d^3r'\rho_B^0(\mathbf{r})\lambda_{BF}^2\chi_F^0(\mathbf{r}-\mathbf{r}')\delta\rho_B(\mathbf{r}'). \tag{19}$$

A comparison of the first and third terms of the right-hand side of Eq. (19) to Eq. (12) indicates that we can associate

$$v_{BB,\mathrm{tot}}(\mathbf{r}-\mathbf{r}') = \lambda_{BB}\delta(\mathbf{r}-\mathbf{r}') + v_{BB,\mathrm{fmed}}(\mathbf{r}-\mathbf{r}') \tag{20}$$

with the linear-response fermion-mediated interaction equal to

$$v_{BB,\mathrm{fmed}}(\mathbf{r}-\mathbf{r}') = \lambda_{BF}^2\chi_F^0(\mathbf{r}-\mathbf{r}'). \tag{21}$$

To determine the fermion-mediated boson-boson energy contribution to the equation of state of the fermion-BEC

mixtures, we integrate the fermion-mediated boson-boson interaction potential over the boson density,

$$E_{BB,\mathrm{fmed}} \approx \int d^3r \int d^3r' \rho_B^0(\mathbf{r}) \frac{v_{BB,\mathrm{fmed}}(\mathbf{r}-\mathbf{r}')}{2} \rho_B^0(\mathbf{r}') = \frac{\lambda_{BF}^2}{2} \chi_F^0(\mathbf{p}\to 0;\omega=0) \frac{N_B^2}{\Omega}, \tag{22}$$

a result that we will obtain rigorously from a perturbation treatment.

While we can evaluate $\chi_F^0(\mathbf{p}\to 0;\omega=0)$ directly from Eq. (17), we can also derive it from the Thomas-Fermi approximation as the static ($\omega\to 0$), long-wavelength ($|\mathbf{k}| \ll k_F$) limit coincides with the regime of validity of the Thomas-Fermi description. In this approximation, we introduce a local Fermi momentum $k_F(\mathbf{r})$ whose local Fermi energy equals the difference of the system's chemical potential and effective Fermion potential energy,

$$\frac{\hbar^2[k_F(\mathbf{r})]^2}{2m_F} = \mu_F - \lambda_{BF}\rho_B^0 - \lambda_{BF}\delta\rho_B(\mathbf{r}). \tag{23}$$

Relative to the equilibrium momentum k_F^0, and its corresponding Fermi energy $\hbar^2(k_F^0)^2/2m_F = \mu_F - \lambda_{BF}\rho_B^0$, the Fermi-momentum variation $\delta k_F(\mathbf{r})$, where $k_F = k_F^0 + \delta k_F$, becomes

$$\delta k_F(\mathbf{r}) \simeq -\frac{m_F}{\hbar^2 k_F^0}\lambda_{BF}\delta\rho_B(\mathbf{r}). \tag{24}$$

Using $\rho_F = k_F^3/(6\pi^2)$, the corresponding linear variation of the fermion density $\delta\rho_F(\mathbf{r})$ is

$$\delta\rho_F(\mathbf{r}) \simeq \frac{(k_F^0)^2}{2\pi^2}\delta k_F(\mathbf{r}) = -\frac{m_F k_F^0}{\hbar^2 2\pi^2}\lambda_{BF}\delta\rho_B(\mathbf{r}), \tag{25}$$

from which we can extract the long-wavelength static density-density response function

$$\lim_{k\to 0}\chi_F^0(\mathbf{k},\omega=0) = -\frac{m_F k_F^0}{\hbar^2 2\pi^2}. \tag{26}$$

With this expression and from Eq. (22), we obtain the fermion-mediated boson-boson interaction energy contribution to the mixture's equation of state,

$$E_{BB,\mathrm{fmed}} = -\lambda_{BF}\frac{N_B^2}{2\Omega}\left(1+\frac{m_F}{m_B}\right)\frac{a_{BF}K_F^0}{\pi}, \tag{27}$$

which gives the fermion-mediated boson-boson interaction energy contribution that is consistent with linear response.

We note that the fermion-mediated energy in Eq. (27) not only arises in response to a boson density variation but also is an integral part of the many-body energy, as we will show in this section.

IV. FERMION-MEDIATED BOSON-BOSON INTERACTIONS IN SECOND-ORDER PERTURBATION

In this section, we determine the fermion-mediated boson-boson interactions using a perturbation approach.

Two assumptions were made. One is that the mixture is homogeneous, i.e., the average densities ρ_B^0 and ρ_F^0 are position-independent, and the other is that the boson-boson scattering length, a_{BB}, is sufficiently small to ensure that the gas parameter $\sqrt{\rho_B^0 a_{BB}^3} \ll 1$ so that the BEC is dilute and well-described by the Bogoliubov approximation. The zeroth order corresponds to the limit $\lambda_{BF}\to 0$ while λ_{BB} remains constant. Thus, the zeroth-order ground state is a product state $|0\rangle = |0\rangle_B \otimes |0\rangle_F$, where $|0\rangle_B$ denotes the weakly interacting BEC ground state, and $|0\rangle_F$ denotes the ground state of an ideal gas of single spin component indistinguishable fermions, corresponding to a filled Fermi sphere of radius k_F. Similarly, the excited states of the zeroth-order Hamiltonian are product states of the zeroth-order fermion ground state and the BEC ground state (or alternatively particle-hole states and boson quasiparticle states).

The perturbation treatment

The perturbation Hamiltonian, $\hat{H}_p$, is the effective interaction potential that describes the short-range boson-fermion interactions,

$$\hat{H}_p = \frac{\lambda_{BF}}{\Omega}\sum_{\mathbf{k}} \hat{\rho}_{\mathbf{k}}^B \hat{\rho}_{-\mathbf{k}}^F, \tag{28}$$

where $\hat{\rho}_{\mathbf{k}}^B$ and $\hat{\rho}_{-\mathbf{k}}^F$ are the momentum Fourier transform of the boson and fermion density operators, respectively.

Using the Bogoliubov approximation for weakly interacting bosons, we write

$$\hat{\rho}_{\mathbf{k}}^B \approx N_B(\hat{c}_{B,\mathbf{k}}^\dagger + \hat{c}_{B,-\mathbf{k}}), \tag{29}$$

where $\hat{c}^\dagger$ ($\hat{c}$) is the boson particle creation (annihilation) operator that is Bogoliubov transformed into a quasiparticle (phonon) operator, $\eta^\dagger$ and η, where $\eta|0\rangle_B = 0$. The Bogoliubov transformation also yields the energy cost of exciting a single quantum of the collective BEC oscillation given by the Bogoliubov dispersion $\hbar\omega_k^B = \hbar kc\sqrt{1+(k\xi)^2}$, where c denotes the sound velocity of the unperturbed BEC, $c = \sqrt{\lambda_{BB}\rho_B^0/m_B}$, and ξ represents its coherence length $\xi = (16\pi\rho_B^0 a_{BB})^{-1/2}$. A direct application of the Bogoliubov transformation also gives the excitation density matrix element,

$${}_B\langle\mathbf{k}|\hat{\rho}_{\mathbf{k}}^B|0\rangle_B = \sqrt{\frac{\hbar^2k^2/2m_B}{\hbar\omega_k^B}}\sqrt{N_B}. \tag{30}$$

The many-body energy can be calculated by expanding the term in the fermion-boson interaction strength,

$$\Delta E = E - E_0 = \Delta E_1 + \Delta E_2 + \cdots, \tag{31}$$

where the jth-order contribution, ΔE_j, varies as $\sim(\lambda_{BF})^j$ as the boson-fermion scattering length is modified.

The first-order energy contribution gives the mean-field fermion-boson interaction energy,

$$\Delta E_1 = {}_B\langle 0|{}_F\langle 0|\hat{H}_p|0\rangle_F|0\rangle_B = \lambda_{BF}\frac{N_B N_F}{\Omega}. \tag{32}$$

Hence, since we can neglect the depletion contribution to the many-body ground state of the zeroth-order BEC (which gives a relative error of order $\sim\sqrt{\rho_B^0 a_{BB}^3}$), the zeroth-order

and first-order energy terms give an equation of state that is identical to the mean-field equation of state. Thus, the perturbation terms of higher order add correlation terms to the mean-field equation of state.

The second-order contribution can be written as the sum over all intermediate states, $|\text{int}\rangle$,

$$\Delta E_2 = -\sum_{|\text{int}\rangle} \frac{|\langle \text{int}|\hat{H}_p|0\rangle|^2}{E_{\text{int}} - E_0}, \tag{33}$$

where E_{int} denotes the corresponding (zeroth-order) excitation energy of the intermediate state. Here we distinguish three kinds of intermediate states: The first category consists of products of the fermion ground state and quasiparticle boson excited states. The second category comprises products of the BEC ground state with particle-hole fermion excited states. The third category consists of products of excited fermion and excited boson states. It is the second category that yields the fermion-mediated boson-boson interaction energy, $\Delta E^{(2)}_{BB,\text{fmed}}$,

$$\Delta E^{(2)}_{BB,\text{fmed}} = -\left(\frac{\lambda_{FB}}{\Omega}\right)^2 \sum_{\mathbf{k},\mathbf{p}} |{}_B\langle 0|\hat{\rho}^B_{\mathbf{k}}|0\rangle_B|^2 \frac{n^F_{\mathbf{p}}(1-n^F_{\mathbf{p}+\mathbf{k}})}{\epsilon^F_{\mathbf{p}+\mathbf{k}} - \epsilon^F_{\mathbf{p}}}, \tag{34}$$

equal to $E_{BB,\text{fmed}}$ in Eq. (22). In the limit where the system size becomes infinite, the matrix element tends to ${}_B\langle 0|\hat{\rho}^B_{\mathbf{k}}|0\rangle_B \to N_B\delta_{\mathbf{k}}$, implying that the corresponding process involves zero momentum transfer. Perhaps because of the zero momentum nature of the momentum transfer processes, this contribution has been left out in other papers [13–15]. Here, we simply mention that this term needs to be included and we show explicitly how the long-wavelength limit corresponds to the infinite size limit of the fermion system.

Consider a large (i.e., a linear size that significantly exceeds the BEC coherence length) but finite-size BEC system immersed in a homogeneous infinite Fermi sea. Then, let the BEC size approach that of the homogeneous fermion system. A finite BEC has a density expectation value ${}_F\langle 0|\hat{\rho}^B_{\mathbf{k}}|0\rangle_B$ that is a smooth function of $\mathbf{k}$. A Fourier transform of the average spatial distribution gives

$${}_F\langle 0|\hat{\rho}^B_{\mathbf{k}}|0\rangle_B = \int d^3r \exp(i\mathbf{k}\cdot\mathbf{r})\rho^0_B(\mathbf{r}). \tag{35}$$

Inserting the expression of Eq. (35) into Eq. (34), we obtain

$$\begin{aligned}\Delta E^{(2)}_{BB,\text{fmed}} &= \int d^3r \int d^3r' \rho^0_B(\mathbf{r})\left(-\lambda^2_{BF}\int \frac{d^3k}{(2\pi)^3}\right. \\ &\quad \left.\times \exp[i\mathbf{k}\cdot(\mathbf{r}-\mathbf{r}')]\frac{1}{\Omega}\sum_{\mathbf{p}} \frac{n^F_{\mathbf{p}}(1-n^F_{\mathbf{p}+\mathbf{k}})}{\epsilon^F_{\mathbf{p}+\mathbf{k}} - \epsilon^F_{\mathbf{k}}}\right)\rho^0_B(\mathbf{r}') \\ &= \int d^3r \int d^3r' \rho^0_B(\mathbf{r}) \frac{V^{(0)}_{BB,\text{fmed}}(\mathbf{r}-\mathbf{r}')}{2}\rho_B(\mathbf{r}'). \end{aligned} \tag{36}$$

This expression is independent of the BEC size and should clearly be included in the many-body energy regardless of the size of the BEC. The infinite BEC limit simplifies the expression by allowing a straightforward substitution to center-of-mass and relative coordinates, equivalent to the long-wavelength limit

$$\langle E^{(0)}_{BB,\text{fmed}}\rangle = -\frac{N_B^2}{2\Omega}\lim_{\mathbf{k}\to 0} v^{(0)}_{BB,\text{fmed}}(\mathbf{k}), \tag{37}$$

where $v^{(0)}_{BB,\text{fmed}}(\mathbf{k})$ is the Fourier transform of $v_{BB,\text{fmed}}(\mathbf{x})$ in Eq. (22).

It is interesting to note that by adding the fermion-mediated boson-boson energy to the mean-field ground-state energy Eq. (2), one obtains an equation of state that exhibits an instability at the same fermion density $\rho_{F,\text{crit}}$ as the mean-field equation of state. However, the instability is not a saddlepoint instability but one of diverging boson compressibility. The boson chemical potential derivative is equal to

$$\begin{aligned}\frac{\partial\mu_B}{\partial\rho_B} &= \lambda_{BB}\left[1-\left(\frac{\lambda_{BF}}{\lambda_{BB}}\right)\left(1+\frac{m_F}{m_B}\right)\frac{k_F a_{FB}}{\pi}\right] \\ &= \lambda_{BB}\left[1-\left(1+\frac{m_F}{m_B}\right)\left(1+\frac{m_B}{m_F}\right)\frac{a_{FB}}{a_{BB}}\frac{a_{BF}k_F}{2\pi}\right],\end{aligned} \tag{38}$$

which vanishes as $\rho_F \to \rho_{F,\text{crit}}$. Since the boson compressibility $\kappa_B = [(\rho^0_B)^2 \partial\mu_B/\partial\rho_B]^{-1}$, the compressibility diverges at that same fermion density. That large values of the compressibility can make a significant impact on the physical behavior of systems is illustrated by the phenomenon of critical opalescence—the sudden increase in light scattering that can turn the appearance of systems milky white near the critical point—which is caused by the increase of density fluctuations that accompanies the large value of the compressibility. In trapped systems, we expect the increase of compressibility to result in higher densities and smaller BEC size. The strikingly different density profile could be an easily detectable "beyond-mean-field" effect.

V. LINKED CLUSTER EXPANSION OF THE GROUND-STATE ENERGY OF FERMION-BOSON MIXTURES

In this section, we develop a linked cluster expansion that complements and extends the above second-order result. The starting point of the expansion is Goldstone's theorem [27], which states that the difference of the exact many-body energy, E, and the zeroth-order energy, E_0, can be written as an infinite sum of zeroth-order ground-state expectation values,

$$E - E_0 = \sum_n \langle 0|\left(\hat{H}_p \frac{1}{\hat{H}_0 - E_0}\right)^n \hat{H}_p|0\rangle_L, \tag{39}$$

where the subscript L indicates that only "linked" diagrams are included (unlinked diagrams factor out to cancel the normalization factor in the denominator). The expectation values of the perturbation Hamiltonian in Eq. (39) are obtained by inserting the completeness relation as a sum over zeroth-order eigenstates in between each perturbation operator, $\hat{H}_p$, and propagator operator, $(\hat{H}_0 - E_0)^{-1}$. Since the bra and ket state matrix elements of the propagator are eigenstates of $\hat{H}_0$, the matrix elements are diagonal and give rise to unperturbed energy denominators. The interaction elements in the numerators (the matrix elements of $\hat{H}_p$) are nondiagonal but are

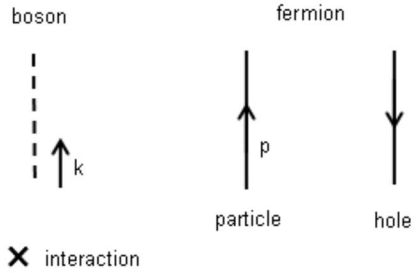

FIG. 2. Symbols and directions used for the diagrams in this paper.

easily calculated. We envision the order in which the operator matrix elements occur to correspond to an effective time ordering (right to left corresponds to increasing "time"). We represent each term of the series of interaction matrix elements and energy denominators (propagators) as a diagram where the effective time parameter runs upwards (see Fig. 2).

In Fig. 3, a "cross," $\times$, denotes a vertex that gives rise to an interaction matrix element. The crosses are connected by fermion and/or boson lines that represent the intermediate states that propagate from one interaction matrix element to another and give rise to an energy denominator. The excited fermion states are represented by solid lines with arrows: upward arrows indicate "particle" states and downward arrows "hole" states. The boson quasiparticle states are represented by dashed lines. Although we do not show the phonon time arrows explicitly in our diagrams, we treat the dashed phonon lines as upward-pointing (boson excitations do not have holes associated with them) when imposing momentum conservation at each vertex (see below). Then the propagator energy denominators are sums over particle-hole fermion excitation energies and boson quasiparticle energies.

Since each application of the $\hat{H}_p$ operator of Eq. (28) creates and annihilates a fermion particle and either creates or annihilates a boson quasiparticle (or gives rise to the diagonal ground-state boson density matrix element), each $\times$ vertex has to have a fermion line that arrives and one that leaves, and each vertex has to have a boson line that either arrives or leaves. The exception to vertices that have a boson line either leaving or arriving are those vertices in which a boson line curves back to make a full circle—a "loop"—

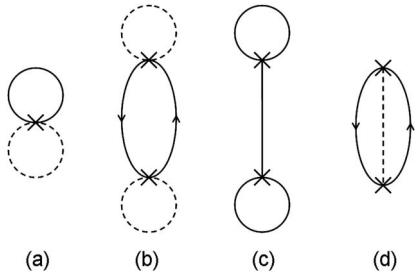

FIG. 3. First- and second-order Goldstone diagrams for a single spin component fermion-boson BEC mixture. (a) Contact interaction, (b) fermion-mediated boson-boson interaction, (c) boson-mediated fermion-fermion interaction (direct term), and (d) boson-mediated fermion-fermion interaction (exchange and polaron terms).

which corresponds to the diagonal ground-state density expectation value ${}_B\langle 0|\hat{\rho}^B|0\rangle_B$ that occurs in the long-wavelength limit arising in the second-order evaluation of the fermion-mediated interaction discussed above. Similarly, a full line that loops back upon the $\times$ vertex that it left from indicates a fermion ground-state matrix element, ${}_F\langle 0|\hat{\rho}^F_{\mathbf{k}}|0\rangle_F \to \delta_{\mathbf{k}} N_F$.

The rules for translating each diagram to a numerical factor are straightforward, so we briefly describe the procedure here. In our case of a homogeneous system, the particle and quasiparticle excitations correspond to good momentum quantum numbers and we assign momentum labels $\mathbf{p}_1, \mathbf{p}_2, \ldots$ to the fermion lines and $\mathbf{k}_1, \mathbf{k}_2, \ldots$ to the boson lines, ensuring conservation of momentum at each $\times$. Next, we divide the vertical "time" axis into separate time intervals between the different interaction $\times$ points and determine the propagator energy denominators to multiply. Converting the remaining sums over boson $\mathbf{k}_j$ and fermion $\mathbf{p}_i$ momenta to dimensionless integrals introduces dimensionless expansion parameters α_F and α_B that quantify the relative importance of fermion and boson excitation induced correlations. Then, we assign a single factor $|\lambda_{BF}|/\Omega$ of the $\hat{H}_p$ operator to each of the momentum summations that remain after enforcing conservation of momentum, and multiply and divide by μ_B^0 for the boson sums and by μ_F^0 for the fermion momentum sums.

After taking the infinite system limit $\Omega^{-1}\Sigma_{\mathbf{k}} \to (2\pi)^{-3}\int d^3k$, we introduce dimensionless momentum variables $\mathbf{k}'_j = \xi \mathbf{k}_j$ for bosons, where $\xi = (16\pi\rho_B^0 a_{BB})^{-1/2}$ is the BEC coherence length, and $\mathbf{p}'_i = \mathbf{p}_i/k_F$, where k_F is the Fermi momentum, and $\hbar^2 k_F^2/(2m_F) = \mu_F^0$. Then integrate over fermion momenta, and write the zeroth-order fermion and boson chemical potentials as μ_F^0 and μ_B^0, respectively.

For boson momentum integrals, we obtain

$$\frac{1}{\mu_B^0}\frac{|\lambda_{BF}|}{\Omega}\sum_{\mathbf{k}} \to \int d^3k \frac{1}{\mu_B^0}\frac{|\lambda_{BF}|}{(2\pi)^3} = \left(\frac{|\lambda_{BF}|\xi^{-3}}{\mu_B^0(2\pi)^2}\right)\frac{1}{2\pi}\int d^3k' = \alpha_B \frac{1}{2\pi}\int d^3k', \tag{40}$$

where α_B denotes the boson expansion parameter

$$\alpha_B = \left(1 + \frac{m_B}{m_F}\right)\frac{2}{\pi}\frac{|\lambda_{BF}|}{\xi}, \tag{41}$$

and for the fermion momentum sum,

$$\frac{1}{\mu_F^0}\frac{|\lambda_{BF}|}{\Omega}\sum_{\mathbf{p}} = \alpha_F \frac{1}{2\pi}\int d^3p', \tag{42}$$

where

$$\alpha_F = \frac{1}{\mu_F^0}\frac{|\lambda_{BF}|k_F^3}{4\pi^2} = \left(1 + \frac{m_F}{m_B}\right)\frac{|a_{FB}|k_F}{\pi}, \tag{43}$$

which plays the role of fermion expansion parameter.

The energy denominators obtained in this procedure contain fermion and boson excitation energies. So, first, we make the denominators positive valued, introducing a -1 factor for each propagator, and verify that particle excitation energies appear with a positive sign and hole excitations with

a negative sign. Then, we make the propagators dimensionless by bringing out an energy scaling factor, μ_F^0 or μ_B^0,

$$\frac{1}{\epsilon^F_{\mathbf{p}_1+\mathbf{p}_2}-\epsilon^F_{\mathbf{p}_2}}=\frac{1}{\mu_F^0}\frac{1}{\mathbf{p}_1'\cdot\mathbf{p}_1+2\mathbf{p}_1'\cdot\mathbf{p}_2'},$$

$$\frac{1}{\epsilon_{\mathbf{k}}}=\frac{1}{2\mu_B^0}\frac{1}{k'\sqrt{1+k'^2}}. \tag{44}$$

For those propagators that contain both boson and fermion excitation energies, we have to choose which energy scale to use. Scaling by the boson chemical potential, we obtain the following expression for the propagator that corresponds to the excited state with one BEC phonon excited of momentum $-\mathbf{k}$, a fermion particle excitation of momentum $\mathbf{p}+\mathbf{k}$, and a fermion hole excitation of momentum $\mathbf{p}$,

$$\frac{1}{\epsilon^B_{-\mathbf{k}}+\epsilon^F_{\mathbf{p}+\mathbf{k}}-\epsilon^F_{\mathbf{p}}}=\frac{1}{2\mu_B^0}\frac{1}{k'\sqrt{1+k'^2}+(m_B/m_F)(\mathbf{k}'\cdot\mathbf{k}'+2\alpha\mathbf{p}'\cdot\mathbf{k}')}, \tag{45}$$

where $\mathbf{k}'\equiv\xi\mathbf{k}$, $\mathbf{p}'\equiv\mathbf{p}/k_F$, and $\alpha\equiv\xi k_F$. Hence, the mixed fermion-boson propagators give rise to dimensionless integrands that depend on the mass ratio (m_F/m_B) as well as on the α parameter that compares the BEC and fermion length scales: $\alpha=2(m_B/m_F)(\alpha_F/\alpha_B)$.

We now include the contributions that stem from the interaction matrix elements. Each fermion loop contributes a factor N_F, each boson loop contributes N_B, and each boson line that connects two vertices and carries a momentum $\mathbf{k}_j$ gives rise to a factor

$$N_B\frac{\hbar^2k_j^2/(2m_B)}{\epsilon^B_{\mathbf{k}_j}}=N_B\left(\frac{k_j'}{\sqrt{1+k_j'^2}}\right). \tag{46}$$

Each fermion hole line of momentum $\mathbf{p}_i$ gives a factor $n^F_{\mathbf{p}_i}$, where n^F denotes the zero-temperature Fermi-Dirac distribution function. In scaled momentum units,

$$n^F_{\mathbf{p}_i}\to n^F_{\mathbf{p}_i'}=\theta(1-|\mathbf{p}_i'|), \tag{47}$$

where θ represents the usual Heaviside function: $\theta(x)=1$ if $x>0$ and $\theta(x)=0$ if $x<0$. Likewise, each upward fermion line of momentum $\mathbf{p}_k$ gives the factor

$$1-n^F_{\mathbf{p}_k}\to 1-n^F_{\mathbf{p}_k'}=\theta(|\mathbf{p}_k'|-1), \tag{48}$$

associated with a particle fermion excitation.

Finally, we have to specify how to take the infinite system (long-wavelength) limit associated with those diagrams that have loops. From the calculation of the fermion-mediated boson-boson interaction in the preceding section, we deduce the following rule: We assign a fictitious momentum $\mathbf{p}_L$ with each fermion loop and a momentum $\mathbf{k}_L$ for the boson loops, conserve momentum at each vertex with this additional momentum, and then take the long-wavelength limits $\lim k_L\to 0$, $\lim p_L\to 0$ at the end of the calculation.

In the next two sections, we use the procedure described above for calculating the equation of state and then analyze the results.

VI. LOW-ORDER DIAGRAMMATIC ANALYSIS

In this section, we briefly describe the first- and second-order contributions to the many-particle ground-state energy of a homogeneous fermion-BEC mixture. Below, we describe the numerical contributions of each diagram shown in Figs. 3(b)–3(d). The derivation of the full expressions is beyond the scope of this paper and will be reported elsewhere. The analysis of this section serves to reveal trends, such as the vanishing of specific diagrams in the low-density BEC limit $\alpha_B\to 0$ in which BEC fluctuation-induced correlations can be neglected.

Much of the challenge in calculating the numerical contributions goes into making judicious choices in dealing with the different ways that the rules can be applied. The labeling of the fermion and boson lines with momenta can be carried out in different ways. For instance, in calculating the contribution of diagram (c), "the bubble diagram with intersecting phonon line," one can either assign a boson momentum $\mathbf{k}$ to the phonon line and a momentum $\mathbf{p}-\mathbf{k}$ to the fermion particle line or one can assign a momentum $\mathbf{p}'$ to the fermion particle line so that the phonon line acquires a momentum $\mathbf{p}-\mathbf{p}'$. The first choice results in an integral over a fermion momentum and an integral over a boson momentum, whereas the second choice results in a double fermion momentum integral. Also, one can scale the mixed fermion-boson energy denominators in the propagators either by the zeroth-order fermion or by the zeroth-order boson chemical potential. Neither of these choices affects the final result, but they can obscure common factors and common limits of different diagrams. For instance, diagrams (b) and (c) give contributions that are equal in magnitude and opposite in sign in the limit $\alpha\to 0$.

We now list and describe the contributions of diagrams (b)–(d). The diagram (b) describes fermion-mediated boson-boson interactions,

$$\Delta E_{(b)}=\Delta E^{(2)}_{BB,\mathrm{fmed}}=-\frac{N_B^2}{2\Omega}\lambda_{FB}\alpha_F=-\frac{N_B^2}{2\Omega}\lambda_{FB}\left(1+\frac{m_F}{m_B}\right)\left|\frac{a_{BF}k_F}{\pi}\right|, \tag{49}$$

obtained earlier in Secs. III and IV. In a Hartree-Fock-like analysis of the boson-mediated fermion-fermion interactions, diagrams (c) and (d) play a special role. Diagram (c) corresponds to the direct part of the boson-mediated interaction,

$$\Delta E_{(c)}=\Delta E^{(2)}_{FF,\mathrm{bmed},D}=-\frac{N_F^2}{2\Omega}\lambda_{FB}\left(\frac{\lambda_{FB}}{\lambda_{BB}}\right), \tag{50}$$

and part of diagram (d) gives the exchange interaction contribution. Specifically, diagram (d) corresponds to the sum of the second-order polaron energy shift experienced by the fermions caused by their interaction with the surrounding BEC phonon fluid and the exchange part of the boson-mediated fermion-fermion interaction,

$$\Delta E_{(d)} = \Delta E^{(2)}_{FF,\mathrm{bmed},X} + \Delta E^{(2)}_{F,\mathrm{med},P}. \tag{51}$$

In a static approximation of the boson-mediated interaction, the fermions attract each other via an attractive Yukawa potential of range ξ. While the static approximation is not always valid, the effective interaction does have an effective range of order ξ so that the α parameter quantifies the ratio of the mediated interaction range to the average fermion-fermion distance. The exchange interaction then depends on the α parameter and the mass ratio (which affects the region in which the static approximation is valid),

$$\Delta E^{(2)}_{FF,\mathrm{bmed},X} = \frac{N_F^2}{2\Omega}\lambda_{FB}\left(\frac{\lambda_{FB}}{\lambda_{BB}}\right)e_X\left(\alpha;\frac{m_F}{m_B}\right). \tag{52}$$

The dimensionless exchange function $e_X(\alpha;m_F/m_B)$ introduced in the above equation satisfies $\lim \alpha\to 0=1$, which ensures that the exchange and direct contributions cancel in the limit that the interaction range is much smaller than the average fermion-fermion distance, as required by the Pauli principle. $\Delta E^{(2)}_{F,\mathrm{med},P}$ denotes the modification to the kinetic energy of ideal fermions with their dispersion altered by the interaction with the surrounding BEC, as described by second-order perturbation theory. This "polaron" contribution is often well described by a zero-momentum energy shift and an effective mass value. For the contact interaction, the second-order polaron contribution has to be renormalized. The resulting energy shift experienced by a single fermion particle is of order $\alpha_B(\lambda_{FB}\rho_B^0)$. The summation over fermion occupation numbers gives a many-body contribution

$$\Delta E^{(2)}_{F,\mathrm{med},P} \simeq N_F\alpha_B(\lambda_{FB}\rho_B^0) = N_B\alpha_B(\lambda_{FB}\rho_F^0), \tag{53}$$

which can be rewritten in the energy units of the boson-mediated interactions using $N_B\alpha_B=(3/2)\alpha^{-3}N_F(\lambda_{FB}/\lambda_{BB})$,

$$\Delta E^{(2)}_{F,\mathrm{med},P} = \frac{N_F^2}{2\Omega}\lambda_{FB}\left(\frac{\lambda_{FB}}{\lambda_{BB}}\right)e_P\left(\alpha;\frac{m_F}{m_B}\right), \tag{54}$$

where the remaining α dependence is absorbed by the dimensionless polarization function e_P. Note that the scale of the boson-mediated fermion-fermion interaction energy per fermion particle is $\lambda_{FB}\rho_F^0$, whereas the scale of the fermion-mediated boson-boson interactions per boson particle is

$$\lambda_{FB}\rho_B^0\alpha_F = \lambda_{FB}\rho_B^0\left(1+\frac{m_F}{m_B}\right)\left(\frac{a_{FB}k_F}{\pi}\right). \tag{55}$$

This also implies that the ratio of the boson-mediated fermion energy scale to the fermion-mediated boson interaction energy is $[\rho_F^0/(\alpha_F\rho_B^0)](\lambda_{BF}/\lambda_{BB})=(8/3\pi)\alpha^2$. In Fig. 4, we show the dimensionless polaron and exchange functions as a function of α for a specific choice of the mass ration $m_F/m_B=6/7$ (corresponding to ^{7}Li-^{6}Li mixtures).

Below, we consider a specific region of the BEC-fermion mixture density space. Starting with a homogeneous mixture of repelling particles ($a_{BB}>0, a_{BF}>0$), comparable fermion and boson densities, and large fermion-boson scattering length (i.e., $a_{BF}\gg a_{BB}$, while still maintaining $a_{BF}k_F\ll 1$), we gradually reduce the boson density. In reducing the number of boson particles to zero, we cannot expect the second-order description of this section to remain valid. A few boson particles cannot mediate interactions for a large number of fermions and give a boson-density independent mediated fermion-fermion interaction. Nevertheless, in the process of decreasing the BEC density, α_F remains constant whereas ξ increases as $\xi(\rho_B^0)^{-1/2}$ so that $\alpha_B\to 0$ and $\alpha\to\infty$ as $\alpha=2(m_B/m_F)(\alpha_F/\alpha_B)$. Notice that in this dilute BEC limit, the contributions of diagram (d) vanish as e_P and e_X rapidly tend to zero as α increases above unity.

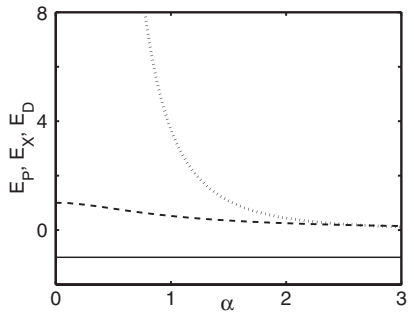

FIG. 4. Direct E_D, exchange E_X, and polaron E_P energies are scaled by $N_F^2/2\Omega\lambda_{FB}(\lambda_{FB}/\lambda_{BB})$ and plotted as a function of α with $m_F/m_B=6/7$.

We could have suspected the vanishing of the diagram (d) contribution as its expression involves a summation over a boson momentum so that we may expect at least a factor α_B. However, the α dependence of the dimensionless integrals complicates the analysis. Nevertheless, the numerical results shown in Fig. 4 confirm the naive expectation of vanishing energy contribution in the dilute BEC limit. This finding indicates a general trend, namely that those diagrams with BEC-phonon momenta that are summed over vanish in the low-density BEC limit. We can expect the diagrammatic analysis to simplify considerably in the dilute BEC region. Even though we consider a low BEC density region, part of this region displays interesting many-body behavior as the fermion-mediated boson-boson attraction competes with the usual contact-interaction boson-boson repulsion.

VII. SUMMATION OF STRETCHED, LINEAR DIAGRAMS

The general diagrammatic analysis becomes unwieldy as the values of the coupling parameters increase. The resulting complexity is a common failing of diagrammatic treatments, often limiting their usefulness in describing strongly interacting systems. Fortunately, in the fermion-BEC mixture, a significant simplification occurs in the low-density BEC limit. For that system, we define the low BEC density regime as the limit in which the BEC is dilute with respect to the usual (contact) boson-boson interactions, $\sqrt{\rho_B^0 a_{BB}^3}\ll 1$, and in which the bosons do not significantly affect the fermion particle properties (altering their effective mass, for instance, or including vertex corrections in the description of effective fermion-boson interactions). The latter conditions are satisfied if

$$\left(1+\frac{m_F}{m_B}\right)\left(1+\frac{m_B}{m_F}\right)\left(\frac{a_{FB}}{a_{BB}}\right)\frac{a_{FB}/\xi}{\pi}\ll 1. \tag{56}$$

In the limit that the fermion-boson interaction is increased, $(1+m_F/m_B)(a_{FB}/a_{BB})\gg 1$, condition (56) is a stronger re-

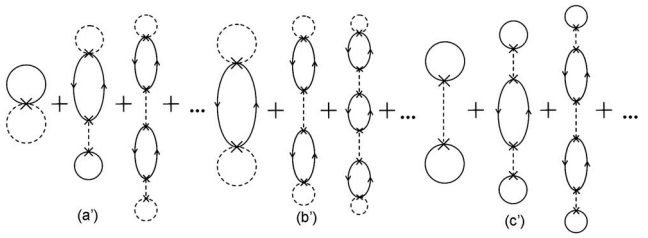

FIG. 5. Higher-order diagrams that are summed.

quirement than $\alpha_B \ll 1$. More generally, diagrams in which phonon momenta have to be summed over can be discarded in this low-density BEC limit. A large class of diagrams is still relevant, however, namely those diagrams in which fermion "bubbles" (particle-hole pairs) are connected by phonon propagators with momenta of vanishing value in the long-wavelength limit implied in loops. This is the case for the diagrams that we will refer to as "linear" diagrams—diagrams with two loops in which one can move linearly from one loop to the other in only one way, crossing all the interaction vertex signs $(\times)$ while passing alternating fermion-bubble and phonon segments.

An important subclass of the linear diagrams is the "stretched" diagrams in which the loops are placed at the earliest and at the latest time and in which the bubble-phonon segments proceed from the earliest to the latest time in a time-ordered fashion, as shown in Fig. 5. The (a′), (b′), and (c′) diagram series shown in that graph follow from Sec. V, (a), (b), and (c) diagrams shown in Fig. 3, by including larger and larger numbers of bubble-phonon insertions in between the loops. Mathematically, each of the next insertions introduces an extra factor $z=(\alpha_F/4)(\lambda_{BF}/\lambda_{BB})$ to the previous term. The z parameter quantifies the magnitude of fermion-mediated boson-boson interactions relative to the usual short-range boson-boson interactions. In the infinite series summation over stretched linear diagrams, z takes on the role of an expansion parameter,

$$z = \frac{\alpha_F}{4}\frac{\lambda_{BF}}{\lambda_{BB}} \tag{57}$$

$$= \left(1+\frac{m_F}{m_B}\right)\left(1+\frac{m_B}{m_F}\right)\frac{a_{BF}k_F}{8\pi}\frac{a_{BF}}{a_{BB}}. \tag{58}$$

The series portrayed in (a′), (b′), and (c′) take on the form $A(1+z+z^2+\cdots)=A/(1-z)$, yielding an equation of state equal to

$$E = \frac{\lambda_{BB}N_B^2}{2\Omega}\left(\frac{1-5z}{1-z}\right) - \frac{\lambda_{BF}N_F^2}{2\Omega}\frac{\lambda_{BF}}{\lambda_{BB}}\left(\frac{1}{1-z}\right) + \frac{\lambda_{BF}N_FN_B}{2\Omega}\left(\frac{1+z}{1-z}\right) + \frac{3}{5}N_F\frac{\hbar^2k_F^2}{2m_F}, \tag{59}$$

where in accordance to the low BEC density limit we have omitted the depletion contribution $(\lambda_{BF}N_F^2/2\Omega)\sqrt{\rho_B a_{BB}^3}$ to the zeroth-order energy E_0. The second-order analysis resulted in a mechanical instability that corresponds to a diverging boson compressibility at a fermion density equal to $z=\frac{1}{4}$ in

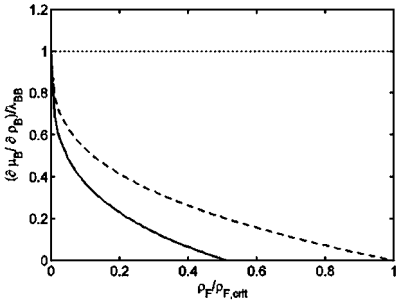

FIG. 6. $(\partial\mu_B/\partial\rho_B)$ (scaled with $\lambda_{BB}T$) is plotted as a function of ρ_F (scaled with $\rho_{B,\mathrm{crit}}$) for mean-field approximation (dotted line), second-order perturbation (dashed line), and infinite summation (solid line).

terms of the new expansion parameter. The present series of stretched linear diagram summation carried out in the low-density BEC limit further shrinks the mechanically stable region to $z<\frac{1}{5}$ as the equation of state of Eq. (59) implies that $\partial\mu_B/\partial\rho_B=\lambda_{BB}(1-5z)/(10z)$. In Fig. 6, we show the boson density derivative of the BEC chemical potential, proportional to the inverse of the boson compressibility, as a function of the fermion density. The density unit on the horizontal axis is $\rho_{F,\mathrm{crit}}$, the critical fermion density calculated in the mean-field and second-order analysis. In the mean-field equation of state, the derivative $\partial\mu_B/\partial\rho_B$ does not depend on the fermion density as this description neglects the fermion-mediated interactions. This result is qualitatively wrong, and in the second-order analysis the derivative does depend on the fermion density but not on the BEC density. Its value vanishes at the fermion density $\rho_{F,\mathrm{crit}}$, corresponding to $z=\frac{1}{4}$. Our low BEC density limit analysis in which we sum over the stretched linear diagrams gives the lowest curve shown in Fig. 6, still depending only on the fermion density and vanishing at a fermion density $\rho_{F,\mathrm{stret}}$ equal to

$$\rho_{F,\mathrm{stret}} = \left(\frac{4}{5}\right)^3 \rho_{F,\mathrm{crit}} \simeq 0.5\rho_{F,\mathrm{crit}}, \tag{60}$$

roughly half of the previous value. We expect that a factor of 2 difference in density should be measurable in cold atom traps.

However, the stretched diagram analysis does not provide a definitive answer even in the low-density BEC limit. So far, we have neglected linear diagrams. The missing Goldstone diagrams can be obtained geometrically by folding the stretched diagrams so as to have time intervals in which multiple excitations occur simultaneously. To judge their importance, we calculate the lowest-order folded linear diagram contributions—the corresponding diagrams are shown in Fig. 3. Their calculation is more involved as some propagators now contain multiple excitation energies. Their combined contribution is equal to

$$\Delta E_{3,\alpha} + \Delta E_{3,\beta} = \lambda_{BF}\frac{N_FN_B}{\Omega}2z\left[1+\left(1-\frac{c}{v_F}\right)\ln\left(1+\frac{v_F}{c}\right)\right]. \tag{61}$$

The simultaneity of phonon and fermion-particle-hole excitations in the diagrams gives rise to a dependence on the

velocity ration $r=c/v_F=m_F/(2m_B\alpha)$. Note that the dependence on fermion and boson numbers is the same as that of the corresponding stretched diagram and so is the order in z, as well as the sign of the contribution (the latter only depends on the order of the diagram).

We expect that the main contributions to the BEC compressibility value stem from the diagrams (b′) of Fig. 5 and their folded versions. The lowest-order folded (b′) diagrams are folded version of the second diagram of the (b′) series—the diagram that has two boson loops, two fermion particle hole bubbles, and one phonon propagator. These fourth-order folded diagrams contribute negative terms to the equation of state and would tend to further lower the value of the fermion density of diverging boson compressibility below $\rho_{F,\mathrm{stret}}$. As their stretched counterpart, they contribute terms that are proportional to N_B^2 and to z^2. Unlike the stretched linear diagram series, these contributions will also depend on the velocity ratio $r=c/v_F$. Hence, we expect them to correct the boson compressibility at order z^2 and higher. The corrections will then give a boson compressibility that depends on not only the fermion density but also on the BEC density. Actually, at very low values of the boson density, this dependence may be significantly affected by other terms as well. Because of the folded diagram r dependence, the third-order diagrams shown in Fig. 5 contribute a term to $\partial\mu_B/\partial\rho_B$ that, for low values of r, $r\ll 1$, varies as $\lambda_{FB}(\rho_B/\rho_F)zr[1-\ln(r)]$. At very low boson densities this term would, in fact, dominate, but since $(\rho_F/\rho_B)(c/v_F)=\sqrt{(8/3\pi)(a_{BB}k_F)}(\rho_F/\rho_B)$, under most experimental conditions, this would happen at BEC densities that would be so low it would be challenging to image their profiles.

VIII. CONCLUSIONS

In this paper, we have developed a perturbation treatment of the zero-temperature equation of state of single spin fermion-boson mixtures with particles that interact via short-range interactions. This study reveals qualitative failings of the mean-field equation of state. For instance, the mechanical instability associated with the spinodal decomposition of the phase-separation transition, which showed up as a saddle-point instability in the mean-field description, turned out to be a point of diverging boson compressibility. A first- and second-order calculation of the equation of state shows that the fermion-mediated boson-boson attraction overcomes the short-range boson-boson repulsion at the same value for the fermion density, $\rho_{F,\mathrm{crit}}$, at which the saddle-point instability occurred in the mean-field analysis. We then showed that in the low BEC density limit, the diagrammatic analysis simplifies to a study of the linear diagrams, of which the "stretched" diagram subclass can be summed, giving an expansion parameter z that quantifies the magnitude of the long-wavelength fermion-mediated interaction relative to the regular short-range boson-boson interactions. The resulting equation of state yields a value of the fermion density at which the boson compressibility diverges that is slightly higher than half corresponding to a factor $(4/5)^3$ of $\rho_{F,\mathrm{crit}}$. A further exploration of the remaining linear diagrams shows that the "folded" diagrams contribute terms that are higher order in z, and we speculate that these contributions will further lower the fermion density at which the mechanical phase-separation instability would set in, giving a critical value of the fermion density that would now depend on the boson density as well. In addition to revealing the inadequacy of the mean-field description near phase separation, these studies have also identified the fermion-mediated interaction as the cause of the mechanical instability associated with the spinodal decomposition of the fermion-boson mixtures. In a general context, the study presented in this paper gives a concrete illustration of how correlations and how the competition of weak interactions can become important near quantum phase transitions in the presence of interactions that, measured by absolute standards, remain weak. The results also suggest that careful experimental measurements near the phase separation transition of fermion-boson mixtures can explore fundamentally interesting quantum many-body behavior.

ACKNOWLEDGMENTS

This work was partly funded by the Laboratory Directed Research and Development (LDRD) program of Los Alamos National Laboratory.

[1] Z. Hadzibabic, C. A. Stan, K. Dieckmann, S. Gupta, M. W. Zwierlein, A. Gorlitz, and W. Ketterle, Phys. Rev. Lett. **88**, 160401 (2002).
[2] K. E. Strecker, G. B. Partridge, and R. G. Hulet, Phys. Rev. Lett. **91**, 080406 (2003).
[3] F. Schreck, L. Khaykovich, K. L. Corwin, G. Ferrari, T. Bourdel, J. Cubizolles, and C. Salomon, Phys. Rev. Lett. **87**, 080403 (2001).
[4] F. M. Cucchietti and E. Timmermans, Phys. Rev. Lett. **96**, 210401 (2006).
[5] L. Viverit, C. J. Pethick, and H. Smith, Phys. Rev. A **61**, 053605 (2000).
[6] D. Pines, *Liquid Helium* (Academic, New York, 1963).
[7] J. M. J. van Leeuwen and E. G. D. Cohen, in *Proceedings of the Eighth International Conference on Low-Temperature Physics*, edited by R. O. Davies (Butterworths Scientific Publications Ltd., London, 1963).
[8] For an overview of the low-temperature helium mixture studies and our current understanding of their many-body structure, see E. Krotscheck and M. Saarela, Phys. Rep. **232**, 1 (1993).
[9] D. Mozyrsky, I. Martin, and E. Timmermans, Phys. Rev. A **76**, 051601(R) (2007).
[10] I. M. Lifshitz and Y. Kagan, Sov. Phys. JETP **35**, 206 (1972).
[11] J. Bardeen, G. Baym, and D. Pines, Phys. Rev. Lett. **17**, 372 (1966).

[12] J. Bardeen, G. Baym, and D. Pines, Phys. Rev. **156**, 207 (1967).
[13] A. P. Albus, F. Illuminati, and M. Wilkens, Phys. Rev. A **67**, 063606 (2003).
[14] A. P. Albus, S. A. Gardiner, F. Illuminati, and M. Wilkens, Phys. Rev. A **65**, 053607 (2002).
[15] L. Viverit and S. Giorgini, Phys. Rev. A **66**, 063604 (2002).
[16] D. V. Efremov and L. Viverit, Phys. Rev. B **65**, 134519 (2002).
[17] A. Bulgac, M. McNeil Forbes, and A. Schwenk, Phys. Rev. Lett. **97**, 020402 (2006).
[18] E. Timmermans, Phys. Rev. Lett. **87**, 240403 (2001).
[19] K. Mølmer, Phys. Rev. Lett. **80**, 1804 (1998).
[20] R. Roth, Phys. Rev. A **66**, 013614 (2002).
[21] G. Modugno, G. Roati, F. Riboli, F. Ferlaino, R. J. Brecha, and M. Inguscio, Science **297**, 2240 (2002).
[22] H. Pu, W. Zhang, M. Wilkens, and P. Meystre, Phys. Rev. Lett. **88**, 070408 (2002).
[23] S. K. Yip, Phys. Rev. A **64**, 023609 (2001).
[24] D. H. Santamore, S. Gaudio, and E. Timmermans, Phys. Rev. Lett. **93**, 250402 (2004).
[25] D. H. Santamore and Eddy Timmermans, Phys. Rev. A **72**, 053601 (2005).
[26] A. Miller and D. Pines, Phys. Rev. **127**, 1452 (1962).
[27] J. Goldstone, Proc. R. Soc. London, Ser. A **A239**, 267 (1957).